*J. Anat.* (2009) **215**, pp227–239 doi: 10.1111/j.1469-7580.2009.01116.x

# Ontogeny of the tessellated skeleton: insight from the skeletal growth of the round stingray *Urobatis halleri*

Mason N. Dean,[1]* Chris G. Mull,[2] Stanislav N. Gorb[3] and Adam P. Summers[1,4]

[1]*Ecology and Evolutionary Biology, University of California Irvine, Irvine CA, USA*
[2]*Department of Biological Sciences, California State University Long Beach, Long Beach, CA, USA*
[3]*Functional Morphology and Biomechanics, Zoological Institute of the University of Kiel, Am Kiel, Germany*
[4]*Friday Harbor Labs, University of Washington, Friday Harbor, WA, USA*

## Abstract

The majority of the skeleton of elasmobranch fishes (sharks, rays and relatives) is tessellated: uncalcified cartilage is overlain by a superficial rind of abutting, mineralized, hexagonal blocks called tesserae. We employed a diversity of imaging techniques on an ontogenetic series of jaw samples to investigate the development of the tessellated skeleton in a stingray (*Urobatis halleri*). We compared these data with the cellular changes that characterize cartilage calcification in bony skeletons. Skeletal growth is characterized by the appearance of tesserae as well as changes in chondrocyte shape, arrangement and density. Yolk sac embryos (35–56 mm disc width, DW) have untessellated lower jaw tissue wrapped in perichondrium and densely packed with chondrocytes. Chondrocyte density decreases dramatically after yolk sac absorption (histotroph stage: 57–80 mm DW) until the formation of tesserae, which are first visible using our techniques as thin (~60 μm), sub-perichondral plaques. During the histotroph stage, flattened chondrocytes align parallel to the perichondrium at the tissue periphery, where we believe they are incorporated into developing tesserae to form the cell-rich laminae observed within tesserae; in older animals peripheral cells in the uncalcified phase are rounder and less uniformly oriented. By parturition (~75 mm DW), cell density and the number of adjoining chondrocyte pairs (an indicator of cell division) have dropped to less than a third of their initial values; these remain low and tesserae continue to grow in size. The tessellated skeleton is a simple solution to the conundrum of growth in an endoskeleton with external mineralization and no remodeling. Although we see parallels with endochondral ossification (e.g. chondrocytes decreasing in density with age), the lack of chondrocyte hypertrophy and the fact that mineralization is sub-perichondral (not the case in mammalian cartilage) suggest that the similarities end there.

**Key words** cartilage; chondrocytes; development; elasmobranch; mineralization; skeletal evolution; tesserae; vertebrate skeleton.

## Introduction

The endoskeleton of elasmobranch fishes (sharks, rays and relatives) is distinct among extant vertebrates for its preponderance of cartilage and the morphology of its mineralization, which suggest an interesting combination of skeletal growth and cartilage calcification pathways. These fishes are called 'cartilaginous' because, unlike most vertebrates, the hyaline-like cartilage of the embryo is not replaced with bone as the animal develops (Applegate, 1967; Moss, 1968; Kemp & Westrin, 1979; Clement, 1992; Dean & Summers, 2006). Whereas vertebrate calcified cartilage is usually a transitional tissue and rarely closely associated with the perichondrium, elasmobranch cartilage possesses a permanent mineralized rind that cannot be remodeled, located beneath the fibrous perichondrium (Fig. 1) (Clement, 1992; Ashhurst, 2004). The distinctive outer layer of calcified cartilage is composed of hexagonal, hydroxyapatite tiles (tesserae; Fig. 1A–C) joined by fibrous tissue (intertesseral joints; Fig. 1D–F) (Dean & Summers, 2006). This tessellated cartilage is found throughout the cranial, appendicular and axial skeleton, except in the vertebral centra, which are formed by appositionally deposited funnels of areolar calcification, nested like ice-cream cones (Ørvig, 1951; Bordat, 1988; Clement, 1992; Dean & Summers, 2006).

Our understanding of the inception and growth of the elasmobranch skeleton is based largely on adult animals, using morphological variation to suggest preceding ontogenetic changes (Schmidt, 1952; Moss, 1968; Applegate,

Correspondence
*Mason Dean, Max Planck Institute of Colloids and Interfaces, Research Campus Golm, 14424 Potsdam, Germany. E: mason.dean@mpikg.mpg.de*

Accepted for publication *26 May 2009*
Article published online *17 July 2009*

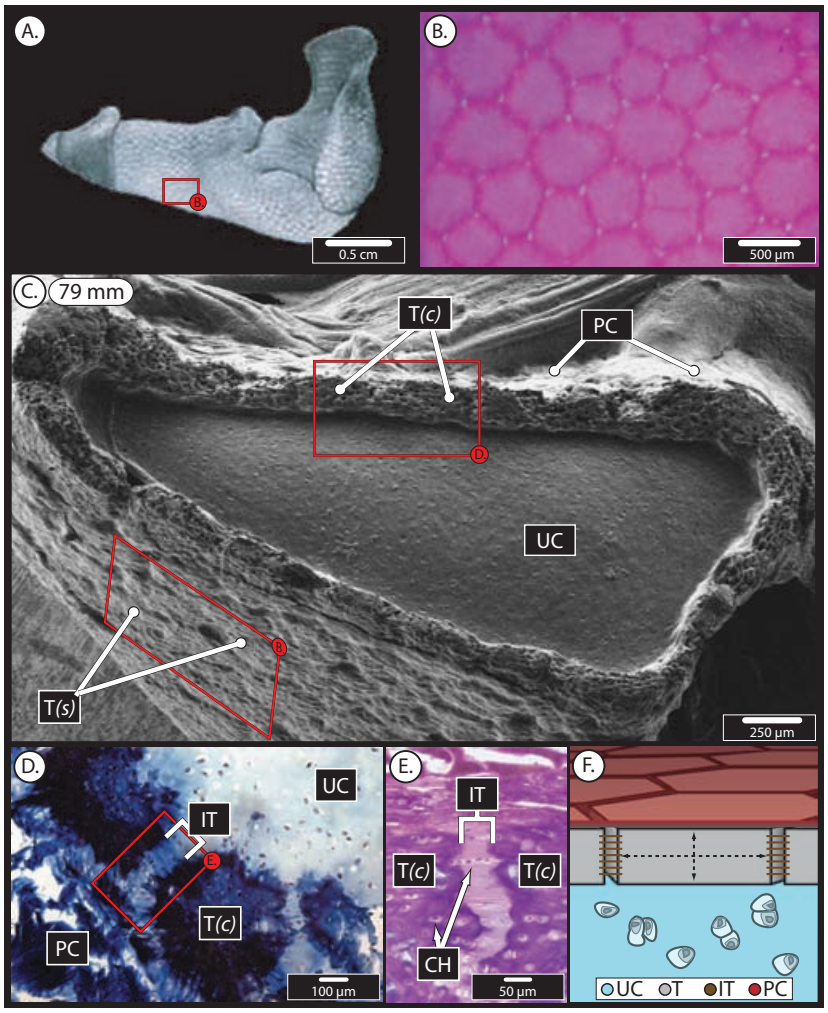


**Fig. 1** Anatomy of the tessellated lower jaw skeleton of batoid elasmobranch fish (stingrays and relatives); lettered and inset red boxes reference other panels in the figure (e.g. the box in panel A references panel B). Elasmobranch skeletal elements are tiled superficially with abutting mineralized blocks called tesserae (T) (panel A: microCT scan, left lateral view; panel B: cleared and stained tissue), overlain by a fibrous perichondrium (PC) and surmounting a monolithic core of uncalcified cartilage (UC; panel C: cryoSEM cross-section). Note the camera view is somewhat oblique in panel C; tesserae can be seen in cross-section [*T(c)*] at the top of the image and in surface view [*T(s)*], covered by perichondrium, at the bottom. This sample was incompletely etched and from a young histotroph animal (79 mm); tesserae are less distinct than in other preparations (see *Methods*). At higher magnifications (panels D, E: hematoxylin-eosin stained cross-sections), the margins of tesserae are less regular and vital chondrocytes (CH) can be seen in mineralized lacunae in tesserae and extending into the intertesseral fibrous joints (IT). The tessellated skeleton can therefore be thought of simply as unmineralized cartilage wrapped in a composite fibro-mineral bark (panel F: schematic cross-section; black arrows indicate dimensions used to determine tesseral width and depth, see *Methods*).

1967; Kemp & Westrin, 1979; Clement, 1992). Nearly all previous studies have focused on the mineralized phase while ignoring the underlying uncalcified tissue (but see Bordat, 1988), which is likely important to the formation of tesserae. The few studies to examine an age series of animals focused on the interaction between the hard and soft tissue phases. Eames et al. (2007) examined changes in the uncalcified matrix leading up to the origin of tesserae, whereas others examined gross changes in the tesserae through calcium marking or mineral content analyses (Applegate, 1967; Doyle, 1968; Boyne, 1970). Bordat (1988) provided a valuable ultrastructural study of tissue changes during growth in the shark *Scyliorhinus canicula*. However, morphological changes were not related back to the animal's natural history (e.g. age of maturity, parturition).

In vertebrates with bony skeletons, cartilage acts as the scaffold on which the majority of osseous tissue is patterned. Skeletal elements begin as cartilaginous precursors and grow in size through an increase in cartilage volume, accomplished by a combination of cell proliferation, deposition of extracellular matrix and enlargement (hypertrophy) of chondrocytes (Hinchliffe & Johnson, 1983; Hunziker, 1992; Wilsman et al. 1996). The relative contribution of each mechanism apparently varies by taxon, but in all cases the population of chondrocytes becomes more strongly heterogeneously organized as the cartilage is gradually calcified and replaced by bone (e.g. Haines, 1934, 1938; Howlett, 1979; Dickson, 1982; Barreto & Wilsman, 1994; Wilsman et al. 1996). In mineralizing tissue, chondrocytes are stratified into discrete zones, exhibiting distinct morphological progressions in cell shape and size from unmineralized to mineralized tissue. Rounded hypertrophic cells are clustered at the mineralization front, often in columns of several cells (chondrones), having transitioned through zones of proliferating chondrocytes from squatter, isolated cells in resting zones further away (Haines, 1934, 1938; Howlett, 1979; Dickson, 1982; Hunziker, 1992; Gerstenfeld & Shapiro, 1996; Schumacher et al. 2002; Youn et al. 2006). In articular tissue, resting chondrocytes are surmounted by a tangential zone of extremely flat cells, oriented parallel to the tissue surface (Paukkonen et al. 1984; Buckwalter et al. 1985; Eggli et al. 1988; Jadin

et al. 2005). Chondrocyte hypertrophy is commonly associated with non-metaplastic cartilage calcification, whether the cells degrade during mineralization (as at the growth plate) or not (as is suggested for cells at the osteochondral junction underlying articular cartilage) (Ali, 1983; Poole et al. 1984; Farnum & Wilsman, 1989; Hunziker, 1992).

Although a roughly similar ontogenetic and mineralization trajectory of cellular changes has been reported for all clades of vertebrates with bony skeletons (e.g. Haines, 1934, 1938; Howlett, 1979; Barreto & Wilsman, 1994; Wilsman et al. 1996), we expect an 'atypical' process in that elasmobranch calcification is superficial and non-transitional (given that no studies have observed changes in cell type or resorption of mineralized tissue). Also, reports disagree as to whether tessellated cartilage exhibits cellular hypertrophy (Peignoux-Deville et al. 1982; Clement, 1992; Egerbacher et al. 2006; Eames et al. 2007) or not (Moss, 1968; Kemp & Westrin, 1979; Ashhurst, 2004; Ortiz-Delgado et al. 2006). A study of elasmobranch skeletal ontogeny will also provide clues to the interaction of calcified and uncalcified tissues (e.g. how vital chondrocytes are incorporated into tesserae) and the generation and maintenance of the tessellated pattern.

Here we examine the ontogeny of tessellated cartilage in an age-series of the round stingray *Urobatis halleri* (Cooper), ranging from yolk sac embryos to mature adults and spanning a more than sixfold change in animal size. We use electron microscopy techniques to look at the development of both phases and the cellular changes that characterize them. We then compare the stingray data with the vertebrate morphological sequence for endochondral ossification to provide a groundwork for understanding the mechanism of growth of the elasmobranch skeleton and the selective pressures that may have shaped its evolution.

## Materials and methods

### Specimens

Haller's round ray is a small, near-shore stingray, common along Central American and southern California coasts. This species was chosen for the extensive published data on its natural history (Babel, 1967; Hale & Lowe, 2008; Mull et al. 2008), its ease of acquisition, and the tractable size of skeletal elements for electron microscopy (see below). The stingrays were collected from monthly beach seines undertaken for age and growth and reproduction research at Seal Beach, California (Hale & Lowe, 2008; Mull et al. 2008). The embryos used in the study were aborted by pregnant females captured in monthly beach seines in the Seal Beach National Wildlife Refuge. Individuals were frozen (–20 °C) immediately following acquisition. Specimens were re-thawed in warm water, their jaws excised and re-frozen. We separated the upper and lower jaws and cleaned them of the majority of muscle and tendinous tissue; however, the thin perichondral wrapping was left intact to avoid damage to the tessellated layer. Efforts were made to reduce the number of thawing events to avoid damage from ice crystallization (Szarko & Bertram, 2006, 2007).

Individuals ($n$ = 19) were collected between July and September 2005 and ranged from yolk sac embryos (35–56 mm disc width, DW; $n$ = 5), to histotroph embryos (57–80 mm DW; $n$ = 4), to subadults (81–150 mm DW; $n$ = 4), to adults (> 150 mm DW; $n$ = 6). Disc width is most commonly used as a size metric for batoid fishes as species in this group vary widely in rostral, standard and total length (Dean et al. 2007). We used males ($n$ = 9) and females ($n$ = 8), as well as two yolk sac embryos (DW < 40 mm) for which sex could not be determined. Differentiation by sex within age classes was precluded by low statistical power; it is likely, however, that sex-based differences are inconsequential in young animals as individuals of both sexes are similar in size before sexual maturity (~150 mm DW) (Hale & Lowe, 2008).

For comparative purposes, we also obtained cow tibial articular cartilage from a local butcher shop (Metzgerei Gungl, Stuttgart, Germany). There are considerable general anatomical data on mammalian articular cartilage; however, as cellular morphometrics vary between age groups and species, and probably between natural and farm-raised animals, this sample was treated as only a rough mammalian benchmark for our stingray data in the contexts of chondrocyte size and orientation (see below). We know of no chondrichthyan chondrocyte data available for comparison.

### Cryo scanning electron microscopy

The boundary between calcified and uncalcified elasmobranch cartilage is abrupt; the stiffness modulus of tesserae is roughly three orders of magnitude greater than the underlying unmineralized phase (Dean, 2007; MN Dean et al. unpubl. data). Because of this, preservation of the interface during sectioning is difficult, and most tissue preparation methods are effective for either one phase or the other, but not both. Previous morphological studies have air-dried, critical point-dried and/or bleached elasmobranch cartilage samples (e.g. Applegate, 1967; Kemp & Westrin, 1979; Dingerkus et al. 1991; Clement, 1992); although these techniques provide clear views of tesserae, they can destroy or distort the native morphology of the unmineralized and fibrous phases.

We developed a low temperature, scanning electron microscopic method for fracturing and viewing elasmobranch cartilage that allows for equal treatment of the tissue phases and planar sectioning of the mineralization front (Dean et al. 2008). As this technique avoids caustic and/or dehydrating methodology, the perichondrium and intertesseral fibers remain in their natural configurations, and chondrocytes and their pericellular tissues are clearly visible throughout, allowing descriptions and quantifications of ultrastructural morphology (Fig. 2). The geometric tessellated pattern on the surface of the skeleton is rendered less obvious in our method (e.g. Fig. 1C) than through critical point drying, bleach treatment, or clearing and staining (as in previous works, e.g. Applegate, 1967; Kemp & Westrin, 1979; Dingerkus et al. 1991; Clement, 1992). However, tesseral margins could be delineated in cross-section by locating fibrous joints (Fig. 2E–F), which appear as parallel-oriented fibers interspersed with cells; these are less distinct in very young tessellated specimens (< 85 mm DW) and samples that have been incompletely etched (Fig. 1C; see below).

We re-thawed each specimen's lower jaw (Meckel's cartilage), bisected it at the symphysis and used a new straight razor blade to trim off the lateral (hyomandibular) and medial (symphyseal) ends of the jaw such that only the middle rectangular (parasymphyseal)

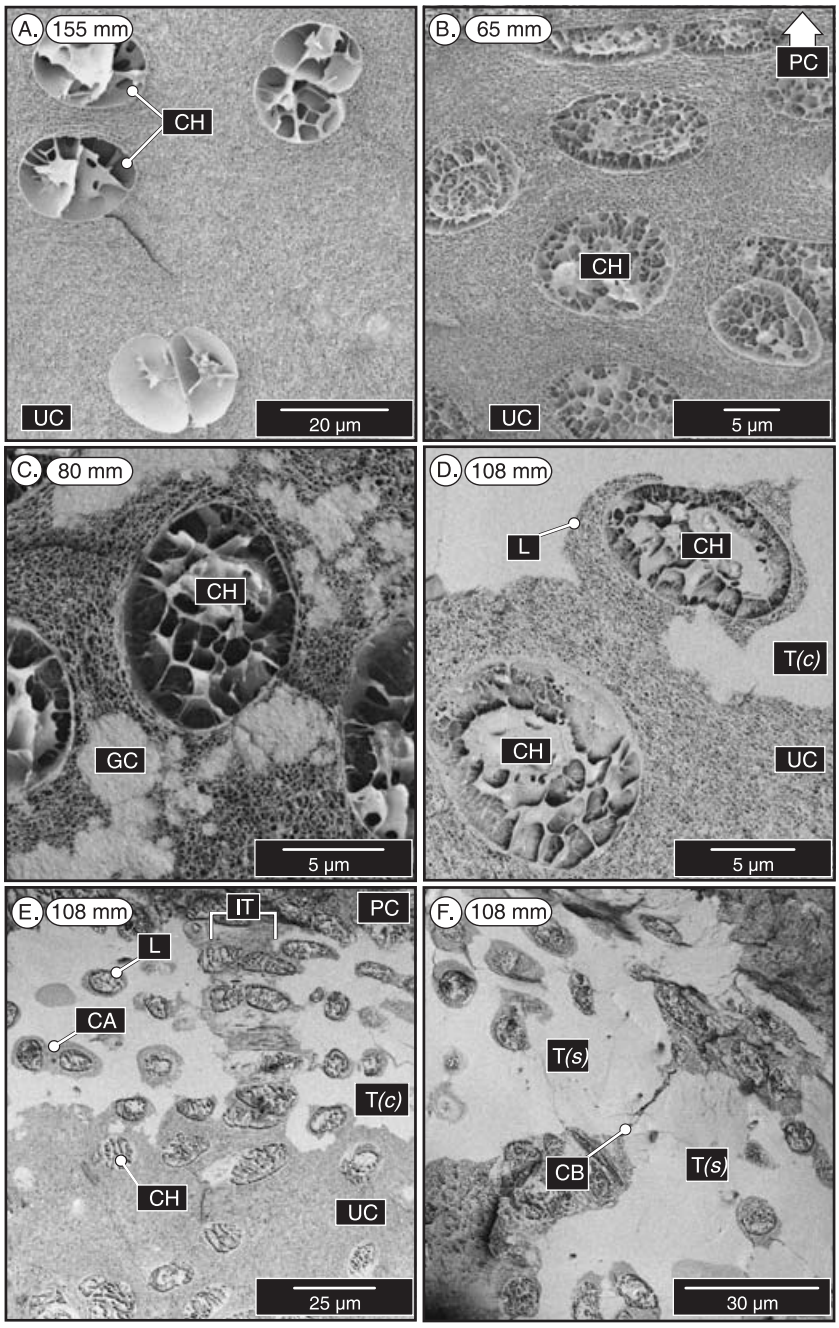


**Fig. 2** Cellular morphometrics in the lower jaw skeleton of the round stingray *Urobatis halleri*; animal size is included in the upper left of each panel. Chondrocytes (CH) in the uncalcified phase exhibit characteristic changes across ontogeny (see Figure 3 and text for full description), such as a decrease in twinning (cell pairing indicative of recent division; panel A) and flattening and orientation relative to the perichondrium (PC; toward the top of the image in panel B). Peripheral chondrocytes appear to be engulfed into forming tesserae (panels C–E), encased in spherulitic blobs of 'globular calcification' (GC) that coalesce (panel C) to form the mineralized walls of lacunae (L; panel D) around chondrocytes. Peripheral cells align end-to-end in 'strings' (see two aligned, flattened cells in panel B), the long axes of which are parallel to perichondral surface (panel E), and are apparently incorporated as a group resulting in cell-rich laminae within tesserae. The pericellular matrix is apparently continuous around cells in a string, communicating through passages (canaliculi, CA) and extending from tesseral centers all the way to the fibrous intertesseral joints (IT), which are also packed with cells (see Fig. 1). In some areas, mineralized cross-bridges (CB; panel F) span the intertesseral space and connect the surface aspects of adjacent tiles. All images were prepared with the cryoSEM technique described in this study and that of Dean et al. (2008); tesserae appear lighter in color because the upper SE detector provides stronger material contrast than the lower one.

portion remained. At least two parasymphyseal cross-sections were performed per animal to account for variation in sample and sectioning quality. The cow specimen was examined from two tissue plugs, approximately 2 × 2 cm and approximately 2 mm deep; chondrocytes observed were well above the osteochondral junction in the resting and proliferative zones and were therefore of average size.

A detailed description of the cryoSEM method can be found in a previous work (Dean et al. 2008). In brief, each specimen was clamped tightly in a cryostub and plunge-frozen in slushed liquid nitrogen before being introduced onto a –140 °C cryostage in the preparation chamber (Gatan Alto 2500) where we cross-sectioned it with a cold scalpel blade with a long, user-controlled handle. The low temperatures ensured a cleaner fracture plane than that obtained in room temperature, resulting in a smooth-faced parasymphyseal cross-section of the lower jaw (Figs 1C, 2). We then etched (sublimated) the sample at –95 °C for 10–15 min to remove the thin surface layer of water and/or contamination by ice crystals, then returned the chamber to its original temperature (–140 °C). We sputter-coated the sample with gold palladium (layer thickness: 6 nm), transferred it to another cryostage in the SEM chamber of the microscope (Hitachi-4800), and visualized it at low accelerating voltage (1–2 kV) at a sample stage temperature of –120 °C. For each cross-section, we captured several digital images at a magnification of ×400 (to quantify cell densities, orientation relative to tesserae and tesseral geometry; see below) and ×1000 (to quantify chondrocyte geometry; see below).

### Chondrocyte and tesserae morphometrics

Chondrocytes and tesserae were hand-traced in Adobe Photoshop CS3 (Adobe Systems, Inc., San Jose, CA) using a Tablet PC (IBM Lenovo ThinkPad X41) and converted into high-contrast black-and-white images. Chondrocyte and tesserae data were collected for bovine tissue and all stingray individuals except the largest individual (220 mm DW), where poor tissue preservation precluded accurate measurement of chondrocytes.

Images were analyzed using a script written for MATLAB v.14 Image Processing Toolbox (The MathWorks, Inc., Natick, MA) to characterize the following descriptors of chondrocytes in the uncalcified matrix: (1) *major axis length* – the length of the longest cell axis; (2) *minor axis length* – the length of the shortest cell axis; (3) *eccentricity* – a scalar describing cell shape, ranging from a perfect circle (0.0) to a line segment (1.0); (4) *chondrocyte density* – the number of chondrocytes per 0.01 $mm^2$ (a $100 \times 100$ μm square), calculated from the cell density within the minimum convex polygon enclosing the cells in the image; (5) *average twin number* – the average number of chondrocyte twins per chondrocyte. 'Twinned' chondrocytes are abutting cells that have recently divided, the number of twins per cell therefore acting as an indirect indication of the cartilage's metabolic activity (Grimshaw & Mason, 2000); twins were defined as those cells within 1.2 minor axis lengths of a focal chondrocyte's centroid. We arrived at this numerical definition through a sensitivity analysis; the distance 1.2 was chosen for its consistent accuracy. Chondrocyte morphometrics for cow tissue were compared with those for stingray and also with published mammalian data to verify that our preparation method was not distorting cells.

We analyzed tesseral geometry using a similar MATLAB script to determine: (6) *average tesseral cross-sectional width* – the linear dimension of a tessera, measured in the plane of the tesseral mat, from one intertesseral edge to the opposite one (Fig. 1F); (7) *average tesseral cross-sectional depth* – the linear distance from the perichondral surface to the chondral surface of each tessera (Fig. 1F). We only analyzed those 'brick-like' (i.e. rectangular) tesserae along the gradually sloping edges of the jaw, as 'corner' tesserae (those at the apex of an acutely angled turn) are less uniform in shape and universal descriptors are difficult (e.g. Fig. 1C, upper left corner of panel). All measurements were taken along the widest point of each tessera. Data were collected from bovine tissue and all stingray individuals larger than the 65 mm DW specimen ($n = 13$); tesserae were not present in individuals smaller than 60 mm DW and although the 65 mm DW jaw was tessellated, tesserae appeared poorly formed and dimensions were difficult to measure accurately in micrographs.

Morphometric data for chondrocytes and tesserae were exported to SigmaPlot 10 (SYSTAT Software, Inc., San Jose, CA) and linearly regressed against disc width. We applied a two-segment piecewise regression to the data for chondrocyte major axis length, density and average twin number to account for pronounced break-points in the data (Kováč et al. 1999). In all cases, we considered changes in the dependent variable to be significantly correlated with disc width where $P > 0.05$.

### Chondrocyte orientation relative to tesserae

In mammalian articular cartilage, flatter chondrocytes are arranged at the periphery of the tissue, parallel to the perichondrium, but mineralization is associated with deeper, rounder chondrocytes (Paukkonen et al. 1984; Hunziker, 1992; Youn et al. 2006; Kronenberg, 2007). To determine whether stingray chondrocytes exhibited shape-bias and/or orientation relative to the mineralization front, we determined chondrocyte eccentricities and the angles of the chondrocyte major axes relative to the base of the nearest tessera (for older stingrays) or the tissue surface (for younger stingrays and the cow sample). To facilitate comparisons, we grouped stingray samples into four age bins: yolk sac embryos, histotroph embryos, sub-adults, and adults (see *Specimens* above for corresponding disc widths). Chondrocyte relative angles (ranging from parallel, 0°, to perpendicular, 90°) and eccentricities were then divided into five distance bins to clarify the distribution of chondrocyte orientations/eccentricities at different distances from the tissue periphery (0–5 μm, 5–10 μm, 10–20 μm, 20–30 μm and 30–40 μm away) and means were compared between bins and age groups. We did not examine chondrocytes further than 40 μm away because in young animals (i.e. smallest skeletal elements) those cells appeared associated with the contralateral perichondral face, and in adults, we found that there was little variation in chondrocyte angle and eccentricity at distances greater than 20 μm (see *Results*). Data were pooled for each individual (stingray and cow) from two ×400 cross-sectional images from that sample. The single bovine sample acts as a rough comparative benchmark for our method, with expected cell orientation angles (< 20°) and eccentricities (> 0.85) based on literature reports of reserve and tangential zone chondrocytes (Paukkonen et al. 1984; Buckwalter et al. 1985; Hunziker, 1992; Jadin et al. 2005; Youn et al. 2006; Kronenberg, 2007).

To determine whether cell orientations and eccentricities differed among groups (stingray age groups and cow), we performed Kruskal–Wallis one-way analysis of variance by ranks tests (SYSTAT Software, Inc., San Jose, CA) for each variable and distance bin; this allowed us to ask whether cell shapes and angles differ among groups at a given distance from the tissue periphery. Where significant differences were detected, we pinpointed the between-group sources of the variation using Dunn's (Q) non-parametric multiple comparison test (Dunn, 1964). Non-parametric rank tests were used to account for unequal sample sizes, the result of lower cell densities in deeper tissues and older animals (see *Results*).

## Results

### Chondrocyte and tesserae morphometrics

All regression analyses showed significant correlation between the means of measured variables and disc widths (Table 1). Tesserae form in histotroph embryos (~60–85 mm DW; see vertical stippled swath running through all panels in Fig. 3; also Fig. 4) at approximately the time of parturition (~75 mm DW; Hale & Lowe, 2008). This is somewhat variable; our cryo-fractured specimens showed well-formed tesserae at disc widths > 65 mm DW, but we have observed cleared and stained specimens of tessellated smaller animals and untessellated larger animals (M. N. Dean, unpubl. data).

The first appearance of tesserae (Fig. 3A) was an important temporal marker, coinciding with changes in chondrocyte distribution and size. Only eccentricity decreased at a consistent rate across our entire ontogenetic series, with tesseral formation having no apparent effect on this

**Table 1** Results of regressions of animal size (disc width, DW) against morphological variables for the round stingray *Urobatis halleri*

| Variable | Regression equation Y = *a*(DW) + *b* | | | | | |
|---|---|---|---|---|---|---|
| | Slope (*a*) | Intercept (*b*) | $r^2$ | *t*-score | *P*-value | Break *(mm DW)* |
| Eccentricity chondrocyte density (cells × 0.01 $mm^{-2}$) | –0.0003 | 0.76 | 0.52 | 4.05 | 0.001 | – |
| *Segment 1* | –1.127 | 113.31 | 0.85 | 10.24 | < 0.0001 | 80.0 |
| *Segment 2* | –0.088 | 30.21 | | | | |
| Chondrocyte major axis (μm) | | | | | | |
| *Segment 1* | –0.079 | 16.05 | 0.70 | 4.59 | < 0.0001 | 56.5 |
| *Segment 2* | 0.035 | 9.64 | | | | |
| Twins (twins per chondrocyte) | | | | | | |
| *Segment 1* | –0.038 | 2.47 | 0.82 | 16.98 | < 0.0001 | 59.9 |
| *Segment 2* | 0.001 | 0.14 | | | | |
| Tesseral depth (μm) | 1.144 | –8.69 | 0.82 | 6.99 | < 0.0001 | – |
| Tesseral width (μm) | 0.891 | 35.98 | 0.83 | 7.27 | < 0.0001 | – |

trend (Fig. 3B); the slight cellular rounding over ontogeny (from 0.75 to 0.70 eccentricity) represents a minor axis length increase of only ~4% of major axis length. Biphasic regressions of cell parameters predicted breakpoints between 56.5 and 80.0 mm DW. On average, prior to tesseral formation, chondrocytes decreased in major axis length from approximately 13 μm (maximum = 24 μm) to 10 μm (maximum = 25 μm; breakpoint = 56.5 mm DW; Fig. 3C) and showed a rapid decrease in density (74 to 23 chondrocytes per 0.01 $mm^2$; breakpoint = 80.0 mm DW; Fig. 3E) from the extremely cell-rich condition of the youngest animals. Similarly, cell division, as indicated by twinning, decreased sharply (1.13 to 0.17 twins per chondrocyte; breakpoint = 59.93 mm DW; Fig. 3D).

Following tesseral formation, chondrocytes increased gradually in major axis length such that adult chondrocytes were on average rounder (0.70; Fig. 3B) and larger (17 μm; maximum = 36 μm; Fig. 3C) than those of yolk sac or histotroph embryos. Concomitantly, chondrocyte density continued to decrease and twin number essentially leveled off such that adult chondrocytes were less densely packed (12 chondrocytes per 0.01 $mm^2$; Fig. 3E) than those of yolk sac or histotroph embryos and showed nearly similar twinning (0.25 twins per chondrocyte; Fig. 3D) as histotroph embryos. We saw no evidence of vertically oriented chondrones (short columns or clusters of three to four cells, oriented perpendicular to the tissue surface) in stingray cartilage.

Tesserae from the jaw of *U. halleri* are predominantly hexagonal in shape and rectangular in cross-section (Figs 1 and 3). Our measurements of tesseral cross-sectional width are proxies for the distance across the perichondral (hexagonal) surfaces of the tesserae. It is impossible to determine if our measurements were made from the vertices or from the edges of the hexagons, therefore our linear measurements should be thought of as mean dimensions for tesserae. Tesserae appeared first as mineralized plaques approximately 130 μm across and 60 μm thick, or half as deep as wide, and then continued to widen and deepen by 2.25–2.75 times from histotroph embryos (79 mm DW) to mature adults (215 mm DW) (Figs 3A and 4). Despite the faster rate of widening (1.14 μm $mm^{-1}$ DW) than deepening (0.89 μm $mm^{-1}$ DW), older tesserae are 'blockier' – roughly two-thirds as deep as wide – and approximately 280 × 180 μm. Overall, the linear dimensions observed for tesserae spanned 60–475 μm across and 35–289 μm deep (Fig. 3A).

On average, bovine chondrocytes were flatter (eccentricity = 0.77 vs. 0.70; Fig. 3B) and smaller (major axis size = 11 μm vs. 17 μm; Fig. 3C) than those of adult stingrays. Although bovine chondrocytes exhibited nearly twice the density of stingray chondrocytes (20 chondrocytes per 0.01 $mm^2$ vs. 12 chondrocytes per 0.01 $mm^2$; Fig. 3E) there were fewer twins per cell (0.06 twins per chondrocyte vs. 0.25 twins per chondrocyte; Fig. 3D), indicating a denser but more even (less clumped) cellular distribution in adult bovine tissue compared with stingray tissue.

## Chondrocyte orientation relative to tesserae

All binwise comparisons exhibited significant differences among groups (Kruskal–Wallis ANOVA; H > 18.0, $P \leq 0.001$). For the most part (across distance bins and age groups), at distances greater than 10 μm away from the periphery, stingray jaw chondrocytes exhibit isotropic orientation relative to the nearest tessera (or perichondrium in yolk sac embryos), with chondrocyte orientation angles between approximately 25° and 40° (Fig. 5). In the band of tissue less than 10 μm from the periphery, cells tend to be flatter (i.e. with higher eccentricities) and oriented at angles more parallel to the tissue surface. This trend is most pronounced in histotroph animals (Fig. 5, column 2), which

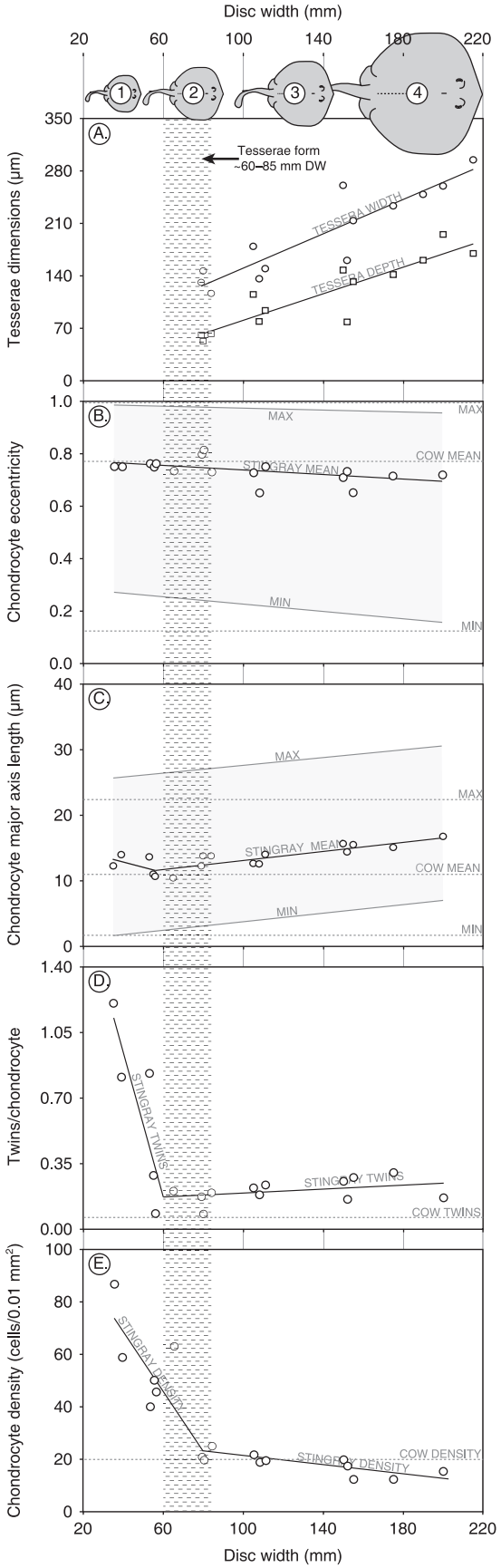


exhibit cells with the lowest orientation angles and highest eccentricities of any age group; this is generally true for all distance bins, but especially noticeable at distances of < 10 μm. These peripheral cells, aligned to the perichondrium, form marginal cell 'strings' (Fig. 2B) often with septa of globular calcification extending between the cells from the undersurface of the adjacent tessera, forming partial or complete mineralized tissue encasements around chondrocytes (Fig. 2C,D).

In general, orientation angles increased and eccentricities decreased (and variation increased for both metrics) with distance from the periphery and as disc widths increased/decreased from the histotroph stage. Therefore, as with our previous cryoSEM data (Figs 2, 3), chondrocyte orientation and eccentricity relative to the periphery are influenced by tesseral formation (late in the histotroph stage; Figs 4 and 5). There was little association of flat chondrocytes with tesserae in adult samples, where only one chondrocyte with eccentricity > 0.75 was found in the nearest distance bin (0–5 μm). By comparison, bovine chondrocytes were consistently flatter and oriented more parallel to the articular surface (and with considerably lower angular and eccentricity variation). The bovine sample always had the highest ranks for eccentricity and lowest ranks for orientation angle in our non-parametric tests; we attribute the similarity among stingray and cow tissue in the deepest distance bin (Fig. 5; right-hand column) to low sample size in the bovine sample (nine cells). Therefore bovine chondrocytes exhibited more pronounced heterogeneity and flattening relative to the periphery, as expected for this tissue (Paukkonen et al. 1984; Buckwalter et al. 1985; Hunziker, 1992; Jadin et al. 2005; Youn et al. 2006; Kronenberg, 2007).

**Fig. 3** Changes in tesseral morphology, chondrocyte geometry and distribution in the Meckel's cartilage of the round stingray *Urobatis halleri* across ontogeny, represented by the four size classes illustrated at the top of the figure. Points represent mean values for each age class; regression statistics can be found in Table 1. Changes were observed from yolk sac embryos (size class 1; 35–56 mm disc width, DW; $n = 5$), to histotroph embryos (size class 2; 57–80 mm DW; $n = 4$), to sub-adults (size class 3; 81–150 mm DW; $n = 4$), to adults (size class 4; > 150 mm DW; $n = 6$). Tesseral formation (marked as the vertical, stippled swath extending through all panels) occurs between 60–85 mm DW (panel A) and is an important inflection point in cellular changes. Leading up to tesseral formation chondrocytes become slightly rounder (panel B; eccentricity values range from a line, 1.0, to a circle, 0.0), decrease in size (panel C), and show rapid decreases in twinning (panel D; see Fig. 1B) and density (panel E). Once tesserae form, they continue to increase in width and depth throughout life (panel A); simultaneously, chondrocytes in the uncalcified phase increase in size, continue to decrease in eccentricity and density, and maintain a roughly constant metabolic activity (as indicated by twinning). Adult stingray values are largely similar to those for adult bovine tissue (means indicated by dashed lines in panels B–D), although cow cells are slightly smaller, flatter and more dense with an apparently overall lower metabolic activity.

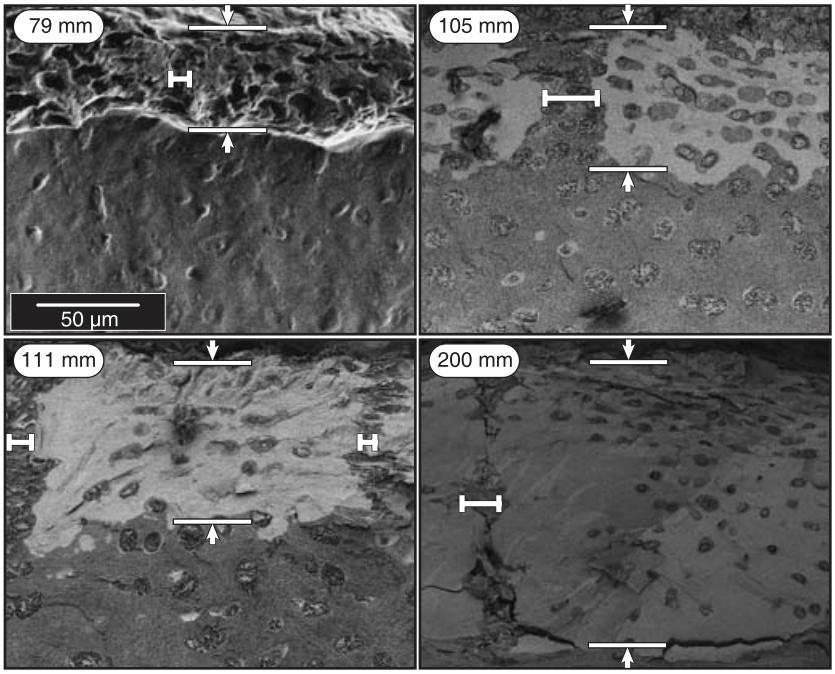


**Fig. 4** Ontogenetic increases in tesseral size in the jaw cartilage of *Urobatis halleri*. Tesserae deepen and widen by ~2.25–2.75 times from their formation in the late histotroph stage through adulthood. The four panels show cross-sections of jaw tesserae arranged in order of increasing animal size (numbers in the upper left corner of each images are disc widths in millimeters). All images are scaled similarly with the perichondral surface at the top of the figure and the chondral surface at the bottom, with arrows indicating the perichondral and chondral surfaces, and therefore the depth of the tesserae. For reference, horizontal white bars indicate tesseral margins and approximate the width of the intertesseral joint at that point; tesserae are less distinct in the first panel due to incomplete etching and young age of the sample (see Fig. 1 and *Methods*).

## Discussion

### Comparative cellular anatomy of cartilage

At the levels of cellular morphology and gross-tissue density, stingray cartilage is not distinct relative to other vertebrate cartilage. Stingray chondrocytes (~10–36 μm) fall within the published size values for vertebrate chondrocytes, which range from 10 μm in articular cartilage up to 30 μm in other cartilages (Kember, 1972; Stockwell, 1978; Kember, 1985). To compare our planar cell densities to volumetric estimates of other studies (as per Stockwell), we can assume cellular density is the same for a two-dimensional section as for the same section extruded by a distance large enough to contain all the observed chondrocytes (two times the average of chondrocyte minor and major axis lengths: 11 μm for stingray and 10 μm for cow tissue). With this conversion, our values for immature ($39.4 \times 10^4$ cells mm$^{-3}$) and adult stingray cartilage ($6.9 \times 10^4$ cells mm$^{-3}$) are within those reported for mammals, which are typically $< 25.0 \times 10^4$ cells mm$^{-3}$ in immature animals and $< 10.0 \times 10^4$ cells mm$^{-3}$ in adults (Rosenthal et al. 1941; Stockwell, 1971, 1978, 1983; Paukkonen et al. 1984; Eggli et al. 1988).

With so little data available on fish (and specifically elasmobranch) chondrocyte morphology and density, it is difficult to know which comparisons with mammalian species and tissues are relevant. Any differences between our bovine and stingray samples may simply reflect differences between adult articular cartilage (cow) and developing non-articular cartilage (stingray); future comparisons between homologous tissues (e.g. developing elasmobranch jaw tissue and developing lateral, non-articular mammalian cartilage) would be valuable. There is huge variation in cell density according to species, cartilage type and tissue location; for example, cartilage cell density varies more than twofold between articular surfaces of the metatarsus, humerus and femur of the rat (from $11.6 \times 10^4$ to $26.5 \times 10^4$ cells mm$^{-3}$), with the femoral densities 5 and 18 times those of femoral densities in sheep and man, respectively (Stockwell, 1971). We note, however, that our data for stingray roughly correspond with the cellular densities and age-related changes reported for small mammals, particularly Rodentia such as rats and rabbits (Stockwell, 1971, 1983). Stockwell (1971, 1978) points to a trend among mammals toward higher densities in younger individuals, smaller taxa and thinner articular cartilage surfaces. Our data also show similar ontogenetic cellular density trends to mammals, including a 22% post-maturity decrease and a sixfold decrease from juveniles to adults (Stockwell, 1967, 1978). This implies similar decreases in elasmobranch and mammalian cartilage metabolism with age and/or similar rates of matrix production despite phylogenetic differences, differences in growth rate (elasmobranch skeletal growth is indeterminate and continues throughout life), and differences in whole animal metabolic rate.

We are confident that our density estimates are accurate, as our bovine cell densities ($9.2 \times 10^4$ cells mm$^{-3}$) fall between those reported for immature ($13.3 \times 10^4$ cells mm$^{-3}$; Rosenthal et al. 1941) and adult ($2.0–4.7 \times 10^4$ cells mm$^{-3}$; Stockwell, 1978) cow articular cartilage. Although this suggests the animal was sub-adult, it is likely an underestimation of

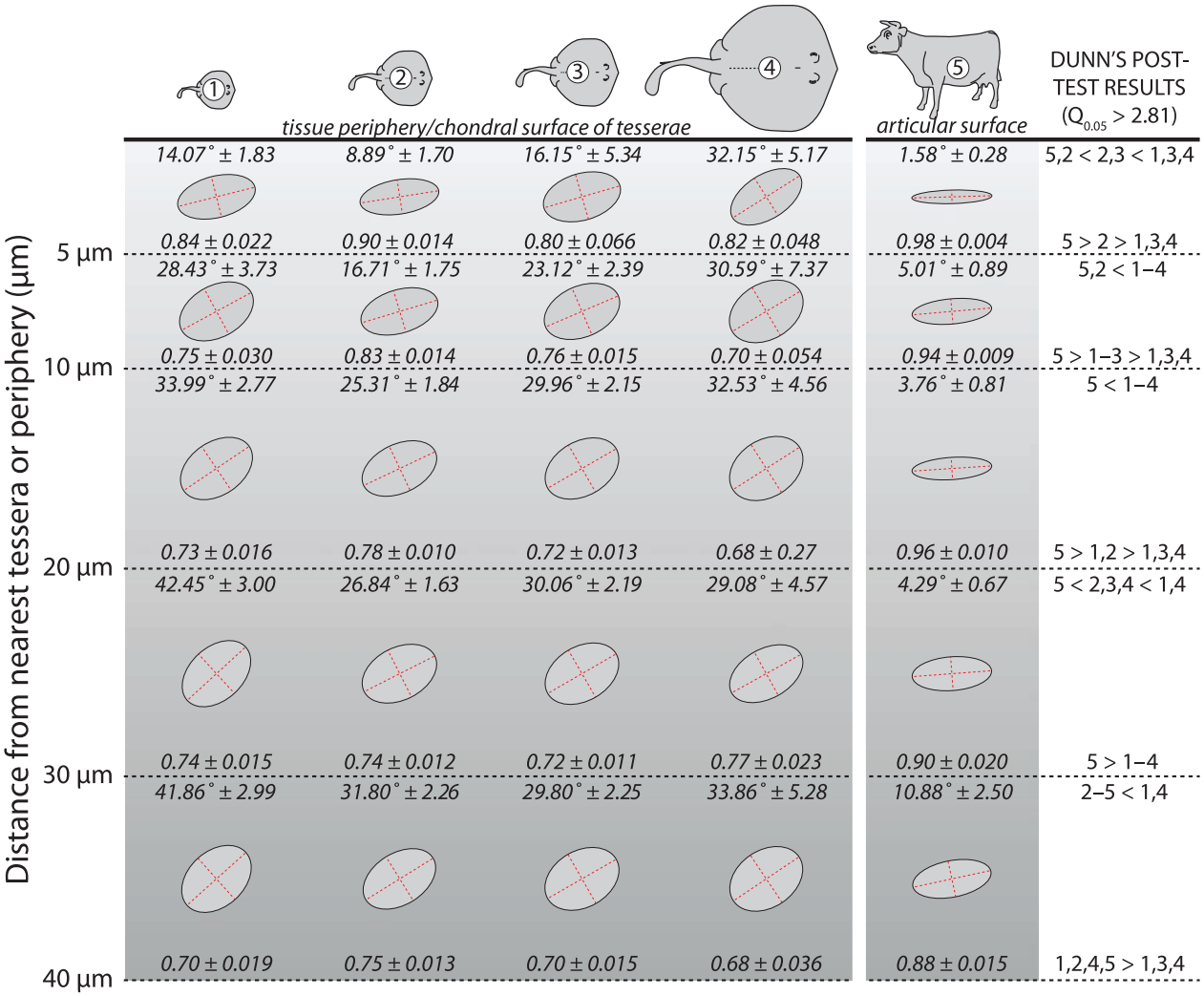


**Fig. 5** Visual and statistical comparisons of chondrocyte eccentricity and orientation angle for stingray age classes (1–4) and cow (5). The *y*-axis rows indicate distance from the tissue periphery (top of the figure), with distance increasing toward the bottom of the figure. Mean orientation angle and eccentricity (± SE) are presented at the top and bottom of each row, respectively. All distance bins show significant differences with a Kruskal–Wallis ANOVA (see *Results*); Dunn's post-test results are presented in the right-hand column, comparing eccentricity and angle among groups for each distance bin ($P \leq 0.05$). For example, in the 10–20 μm bin, cow orientation angles are smaller (cells are more parallel to the periphery) than those for all stingrays, which do not differ from each other; cow chondrocytes are also flatter than yolk-histotroph cells, which are flatter than yolk-sub-adult-adult cells. Visual representations of cells are scaled according to mean chondrocyte angles and eccentricities.

densities because our bovine sections did not include the comparatively cell-dense deep tissue regions. The similarities between our data on cell geometries (stingray and bovine) and distributions and literature values support our use of two-dimensional cryo-sections for description of tissue morphology.

### Cellular zones

Chondrocytes play a large role in endochondral ossification and also apparently in elasmobranch cartilage calcification, as the most profound changes in chondrocyte morphology coincide with tesseral formation (Figs 2, 3, 5 and 6). We treat tessellation as the start of large-scale skeletal mineralization, although the true onset of calcification is surely earlier and more subtle, as suggested by localized alkaline phosphatase activity that precedes tesserae formation in the swell shark, *Cephaloscyllium ventriosum* (Eames et al. 2007). During endochondral ossification, mammalian chondrocytes undergo a characteristic process of spatial organization and orientation, proliferation and hypertrophy, after which the post-mitotic chondrocytes are involved in decomposition, removal, and degradation of matrix material to lay the groundwork for mineral nucleation (Ali, 1983; Poole et al. 1989; Guilak et al. 1995; Kronenberg, 2007).

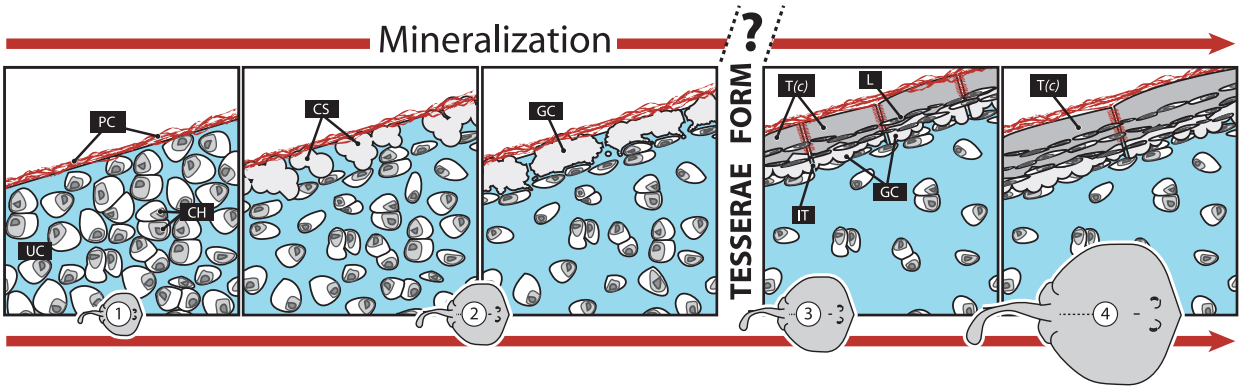


**Fig. 6** Composite hypothesis of elasmobranch mineralization based on the present study of *Urobatis halleri* and previous works (see *Discussion*). Stingray age classes are included at the bottom of the image for reference with age increasing from left to right. In early embryos, the uncalcified matrix (UC) is extremely rich in chondrocytes (CH), which are likely involved in altering the matrix directly beneath the perichondrium (PC) to facilitate mineralization (see *Discussion*). Calcium phosphate precipitation occurs in spherulitic calcospherites (CS), globular calcifications (GC) that coalesce in isolated sub-perichondral plaques, their locations predicted by alkaline phosphatase activity and perhaps the intersections of fiber bundles in the perichondrium. The morphology of the earliest tesserae is unknown, but once tesserae form (shown in cross-section, T*(c)*), they accrete mineral on all surfaces and continue to both widen and deepen with age. Tesserae thicken by engulfing chondrocytes in their lacunae (L) on their chondral surfaces while laying down perichondral mineral peripherally. Simultaneously, tesserae grow wider by mineral deposition on the abutting surfaces of intertesseral joints (IT). Although tesserae form in the jaws of *U. halleri* at approximately the time of parturition, this timing likely varies considerably across body regions and species.

By contrast, stingray jaw cartilage mineralization is associated with flattened peripheral chondrocytes rather than deep, hypertrophied cells (Figs 5 and 6). The factors involved in the first formation of tesserae could not be determined with our methods and represent a fertile area for future work; however, we expect the peripheral flattening of chondrocytes during tesseral development to coincide with up-regulation of alkaline phosphatase in marginal tissue (Eames et al. 2007) and additional changes in matrix chemistry, wherein cells would either synthesize substances to initiate calcium precipitation or cease production of substances that prevent mineralization (Poole et al. 1989; Kronenberg, 2007). Clement (1992) argued that the elasmobranch mineralization pathway closely mimics endochondral ossification in mammals, but obviates the final 'two steps in the process' where calcified cartilage is removed and replaced by bone (p. 176). However, we find little similarity between the processes at the level of cellular distributions. If anything, the elasmobranch cartilage plan is roughly similar to only the most superficial mammalian strata – the tangential and resting zones – where flatter cells are more peripheral and with an anisotropic orientation relative to the tissue surface (Poole et al. 1982; Ali, 1983; Guilak et al. 1995; Wong & Carter, 2003; Jadin et al. 2005; Youn et al. 2006; Kronenberg, 2007). These 'zones' are far less distinct in *U. halleri* than in other taxa: the tangential mineralizing zone (i.e. region of flattened cells) is not only very narrow (~1 cell major axis deep) and comprised of comparatively rounder cells (mammalian tangential cells can attain eccentricities of nearly 1.0), but apparently transient, as the zone is only distinct in the histotroph stage (Figs 5 and 6). This may be related to the apparent whole-tissue decreases in cell division and cell density. As flattened cells were arranged in 'strings' parallel to forming tesserae (see *Results* and Fig. 2), it is possible that peripheral chondrocytes are clustered into horizontal chondrones, as in superficial cells for some mammalian articular cartilages (Schumacher et al. 2002), but this was difficult to verify with our two-dimensional method. Our images showing peripheral cells partially surrounded by globular calcification support assertions that tesserae engulf cells from the uncalcified tissue below (e.g. Clement, 1992; Kemp & Westrin, 1979), and our illustration of an aligned marginal layer suggests that the cellular laminae in tesserae are formed by wholesale engulfment of entire cell strings.

We agree with previous authors in noting a complete lack of cellular hypertrophy in jaw tissue (Kemp & Westrin, 1979; Moss, 1968); mammalian hypertrophic chondrocytes are dramatically larger and rounder than superficial cells, with eccentricities as low as 0.3 in the lower hypertrophic zone (Buckwalter et al. 1985). It is the 'rounding' of chondrocytes (the 4–10 times increase in height during hypertrophication) that contributes to skeletal growth in mammalian tissue (Buckwalter et al. 1986; Farnum & Wilsman, 1989). In contrast, stingray jaw chondrocytes at most tissue depths are oblate spheroids with eccentricities on average between 0.68 and 0.85 (Fig. 5). Calcification of elasmobranch jaw cartilage apparently does not involve chondrocyte hypertrophy and therefore may be a unique case among vertebrate cartilage mineralization pathways. The lack of hypertrophy also suggests that growth of

stingray jaw cartilage is largely a function of matrix deposition and cell proliferation and the ontogenetic decrease in the latter (evidenced by a decrease in the number of twins per cell) represents an increase in the prevalence of the former in older animals. If this is the case, the engulfing of marginal chondrocytes by tesserae effectively reduces the population of matrix-producing cells (assuming tesseral chondrocytes, encased in mineral, are no longer contributing matrix material to the underlying uncalcified phase) and also perhaps restricts signals between the perichondrium and underlying uncalcified cartilage (Kronenberg, 2007); labeling and cell-fate studies will provide insight into the balance of growth and mineralization processes in this tissue.

### Tesseral growth

We have shown that, once calcification has begun, tesserae enlarge in both depth and width as hypothesized by previous authors (Benzer, 1944; Schmidt, 1952; Kemp & Westrin, 1979). Following tesseral formation, cell density continues to fall, though at a slower rate than in the pretesseral phase, and the peripheral distribution and orientation of flattened chondrocytes becomes less dramatic. Assuming a link between the peripheral orientation/organization of cells and the adjacent mineralization process, this suggests a decreased prevalence of chondral-surface mineralization of tesserae with age; however, Schmidt (1952) argued from morphological observations that the developmental centers of pectoral fin tesserae are closest to the superficial face, and therefore perichondral growth is much 'weaker' than accretion on lateral or chondral surfaces. It is possible that mechanisms and rates of tesseral growth vary throughout the body; our preliminary data from calcium-labeled animals suggests that neural arch tesserae grow faster than jaw tesserae (Dean et al. *in preparation*). We therefore caution against the assumption that our tesseral growth rates are universal across species and even within the body of a single animal.

However, we do suppose – given the nature of cartilage growth and the peripheral location of mineral in elasmobranch skeletons – that all tesserae accrete mineral on all surfaces and continue to increase in size and mineral content with age (Doyle, 1968; this study). Cartilage is avascular and aneural and both the mineralized and unmineralized elasmobranch cartilages are incapable of remodeling (Clement, 1992; Ashhurst, 2004; Hall, 2005). Elasmobranch skeletons, unlike bony ones, are therefore 'deposition-only'. It is easy to imagine a non-remodeling skeleton that grows, concentrically accreting mineral on its outer surface only: the final skeletal element is the result of accreted previous versions, nested like a set of Russian matryoshka dolls. Without remodeling, this mechanism is only effective in conditions where the volume of the central cavity is static or decreasing. However, we know that in the tessellated skeleton both tissue phases increase in volume with age (this study; Doyle, 1968; Bordat, 1988; Dingerkus et al. 1991; Fahle & Thomason, 2008).

We therefore posit that the tessellated surface pattern of the elasmobranch skeleton is a key feature that allows growth without remodeling. An increase in the volume of the uncalcified cartilage core of an elasmobranch skeletal element would be impossible with a shell that could not repair/resorb and was continuous. An increase in the volume of both phases is only possible if mineralized tissue can be deposited interstitially; tessellation of the mineralized layer allows for this. In an untessellated system, the proportion of uncalcified to calcified material would quickly decrease; this would likely have profound mechanical implications as it is the proportionate mixing of the two cartilage phases that imparts the combination of high stiffness and high damping capacity to tessellated cartilage (Dean et al. 2009).

### Concluding remarks

Tessellation and growth of the jaw cartilage of the round stingray *U. halleri* are characterized by changes in chondrocyte morphology, orientation and distribution, but without the strong zonal variation of chondrocytes seen in vertebrates with predominantly bony skeletons. Tessellated cartilage growth is made possible by an early organization of isolated, surface mineralization centers that grow appositionally to maintain contact as the underlying uncalcified matrix expands in volume. The tessellated skeleton is therefore an elegant solution to the problem of skeletal growth with continued integrity but without resorption or remodeling. Although the mineralization process may share some basic similarities with mammalian endochondral calcification in terms of cell organization (e.g. alignment of flattened chondrocytes at the tissue periphery) and perhaps matrix reorganization (e.g. the expression of alkaline phosphatase and reduced sulfation in zones of mineralization; Doyle, 1968; Takagi et al. 1984; Gelsleichter et al. 1995; Eames et al. 2007; Egerbacher et al. 2006), we believe the similarities to end there. We hope that future work on the growth mechanism of the tessellated skeleton will focus on the respective roles of the populations of cells involved, and the regulation and localization of mineral deposition that result in the maintenance of such close association of mineralized and unmineralized tissues. This may provide insight into the initial evolution of the perichondral mineralization program, which predated the evolution of jaws (Donoghue & Sansom, 2002).

## Acknowledgements

We would like to thank Chris Lowe, Lori Hale and the CSULB Shark Lab for unwavering generosity and specimens. Lena Gorb, Connie

Miksch, Jan Schuppert, Matt Szarko and Dagmar Voigt were instrumental in developing and troubleshooting the cryoSEM technique; Joe Bizzarro, Malcolm Francis, Lara Ferry-Graham and Mike Graham guided our statistical analysis; Brian Eames, Tamara Franz-Odendaal, Farsh Guilak, Jason Ramsay and P. Eckhard Witten provided invaluable comparative insight into non-batoid systems. We would also like to thank the Department of Ecology & Evolutionary Biology and Biomechanics Lab of the University of California Irvine for their continual support and input. This research was supported by a National Science Foundation grant to M.N.D. and A.P.S. (IOB-0616322), and Journal of Experimental Biology Traveling and University of California Irvine Chancellor's Club fellowships to M.N.D.

## References

**Ali SY** (1983) Calcification of cartilage. In *Cartilage* (ed. Hall BK), pp. 343–378. New York: Academic Press.

**Applegate SP** (1967) A survey of shark hard parts. In *Sharks, Skates and Rays* (eds Gilbert PW, Mathewson RF, Rall DP), pp. 37–66. Baltimore: Johns Hopkins Press.

**Ashhurst DE** (2004) The cartilaginous skeleton of an elasmobranch fish does not heal. *Matrix Biol* **23**, 15–22.

**Babel JS** (1967) Reproduction, life history, and ecology of the round stingray, *Urolophus halleri* Cooper. *Fisheries Bull* **137**, 1–104.

**Barreto C, Wilsman NJ** (1994) Hypertrophic chondrocyte volume and growth-rates in avian growth plates. *Res Vet Sci* **56**, 53–61.

**Benzer P** (1944) Morphology of calcification of *Squalus acanthias*. *Copeia* **4**, 217–224.

**Bordat C** (1988) Les cartilages calcifiés de la petite roussette (*Scyliorhinus canicula* L., Chondrichthyens): Histologie et ultrastructure. *Can J Zool-Rev Can Zool* **66**, 1432–1445.

**Boyne PJ** (1970) Study of the chronologic development and eruption of teeth in elasmobranchs. *J Dent Res* **49**, 556–560.

**Buckwalter JA, Mower D, Schafer J, Ungar R, Ginsberg B, Moore K** (1985) Growth-plate-chondrocyte profiles and their orientation. *J Bone Joint Surg Am* **67A**, 942–955.

**Buckwalter JA, Mower D, Ungar R, Schaeffer J, Ginsberg B** (1986) Morphometric analysis of chondrocyte hypertrophy. *J Bone Joint Surg Am* **68A**, 243–255.

**Clement JG** (1992) Re-examination of the fine structure of endoskeletal mineralization in Chondricthyes: implications for growth, ageing and calcium homeostasis. *Aust J Mar Freshwater Res* **43**, 157–181.

**Dean M** (2007) Ontogeny, morphology and mechanics of the tessellated skeleton of cartilaginous fishes. *J Morphol* **268**, 1066.

**Dean MN, Summers AP** (2006) Cartilage in the skeleton of cartilaginous fishes. *Zoology* **109**, 164–168.

**Dean MN, Bizzarro JJ, Summers AP** (2007) The evolution of cranial design, diet, and feeding mechanisms in batoid fishes. *Integr Comp Biol* **47**, 70–81.

**Dean MN, Gorb SN, Summers AP** (2008) A cryoSEM method for preservation and visualization of calcified shark cartilage (and other stubborn heterogeneous skeletal tissues). *Micros Today* **16**, 48–50.

**Dean MN, Youssefpour H, Earthman JC, Gorb SN, Summers AP** (2009) Micro-mechanics and material properties of the tessellated skeleton of cartilaginous fishes. *Integr Comp Biol* **49**, e45.

**Dickson GR** (1982) Ultrastructure of growth cartilage in the proximal femur of the frog, *Rana temporaria*. *J Anat* **135**, 549–564.

**Dingerkus G, Séret B, Guilbert E** (1991) Multiple prismatic calcium phosphate layers in the jaws of present-day sharks (Chondrichthyes; Selachii). *Experientia* **47**, 38–40.

**Donoghue PC, Sansom I** (2002) Origin and early evolution of vertebrate skeletonization. *Micros Res Tech* **59**, 352–372.

**Doyle J** (1968) Ageing changes in cartilage from *Squalus acanthias* L. *Comp Biochem Physiol* **25**, 201–206.

**Dunn OJ** (1964) Multiple comparisons using rank sums. *Technometrics* **6**, 241–252.

**Eames BF, Allen N, Young J, Kaplan A, Helms JA, Schneider RA** (2007) Skeletogenesis in the swell shark Cephaloscyllium ventriosum. *J Anat* **210**, 542–554.

**Egerbacher M, Helmreich M, Mayrhofer E, Böck P** (2006) Mineralisation of the hyaline cartilage in the small-spotted dogfish *Scyliorhinus canicula* L. *Scripta Medica (BRNO)* **79**, 199–212.

**Eggli PS, Hunziker EB, Schenk RK** (1988) Quantitation of structural features characterizing weight-bearing and less-weight-bearing regions in articular-cartilage – a stereological analysis of medial femoral condyles in young-adult rabbits. *Anat Rec* **222**, 217–227.

**Fahle SR, Thomason JC** (2008) Measurement of jaw viscoelasticity in newborn and adult lesser spotted dogfish *Scyliorhinus canicula* (L., 1758). *J Fish Biol* **72**, 1553–1557.

**Farnum CE, Wilsman NJ** (1989) Condensation of hypertrophic chondrocytes at the chondro-osseous junction of growth plate cartilage in Yucatan swine – relationship to long-bone growth. *Am J Anat* **186**, 346–358.

**Gelsleichter JJ, Musick JA, van Veld P** (1995) Proteoglycans from the vertebral cartilage of the clearnose skate, *Raja eglanteria* – inhibition of hydroxyapatite formation. *Fish Physiol Biochem* **14**, 247–251.

**Gerstenfeld LC, Shapiro FD** (1996) Expression of bone-specific genes by hypertrophic chondrocytes: Implications of the complex functions of the hypertrophic chondrocyte during endochondral bone development. *J Cell Biochem* **62**, 1–9.

**Grimshaw MJ, Mason RM** (2000) Bovine articular chondrocyte function in vitro depends upon oxygen tension. *Osteoarthritis Cartilage* **8**, 386–392.

**Guilak F, Ratcliffe A, Mow VC** (1995) Chondrocyte deformation and local tissue strain in articular cartilage – a confocal microscopy study. *J Orthop Res* **13**, 410–421.

**Haines RW** (1938) The primitive form of epiphysis in the long bones of tetrapods. *J Anat* **72**, 323–343.

**Haines WR** (1934) Epiphysial growth in the branchial skeleton of fishes. *Q J Microsc Sci* **77**, 77–97.

**Hale LF, Lowe CG** (2008) Age and growth of the round stingray, *Urobatis halleri* at Seal Beach, California. *J Fish Biol* **73**, 510–523.

**Hall BK** (2005) *Bones and Cartilage: Developmental Skeletal Biology*, London: Elsevier/Academic Press.

**Hinchliffe JR, Johnson DR** (1983) Growth of cartilage. In *Cartilage* (ed. Hall BK), pp. 255–295. New York: Academic Press.

**Howlett CR** (1979) Fine-structure of the proximal growth plate of the avian tibia. *J Anat* **128**, 377–399.

**Hunziker EB** (1992) Articular cartilage structure in humans and experimental animals. In *Articular Cartilage and Osteoarthritis* (eds Kuettner K, Schleyerbach R, Peyron JG, Hascall VC), pp. 183–199. New York: Raven Press.

**Jadin KD, Wong BL, Bae WC, et al.** (2005) Depth-varying density and organization of chondrocytes in immature and mature bovine articular cartilage assessed by 3D imaging and analysis. *J Histochem Cytochem* **53**, 1109–1119.

**Kember NF** (1972) Comparative patterns of cell division in epiphyseal cartilage plates in the rat. *J Anat* **111**, 137–142.

**Kember NF** (1985) Comparative patterns of cell division in epiphyseal cartilage plates in the rabbit. *J Anat* **142**, 185–190.

**Kemp NE, Westrin SK** (1979) Ultrastructure of calcified cartilage in the endoskeletal tesserae of sharks. *J Morphol* **160**, 75–102.

**Kováč V, Copp GH, Francis MP** (1999) Morphometry of the stone loach, *Barbatula barbatula*: Do mensural characters reflect the species' life history thresholds? *Environ Biol Fishes* **56**, 105–115.

**Kronenberg HM** (2007) The role of the perichondrium in fetal bone development. *Ann N Y Acad Sci* **1116**, 59–64.

**Moss M** (1968) The origin of vertebrate calcified tissues. In *Current Problems of Lower Vertebrate Phylogeny* (ed. Ørvig T), pp. 373–397. Stockholm: Almqvist and Wiksell.

**Mull CG, Lowe CG, Young KA** (2008) Photoperiod and water temperature regulation of seasonal reproduction in male round stingrays (*Urobatis halleri*). *Comp Biochem Physiol A Physiol* **151**, 717–725.

**Ortiz-Delgado JB, Simes DC, Viegas CSB, Schaff BJ, Sarasquete C, Cancela ML** (2006) Cloning of matrix Gla protein in a marine cartilaginous fish, *Prionace glauca*: preferential protein accumulation in skeletal and vascular systems. *Histochem Cell Biol* **126**, 89–101.

**Ørvig T** (1951) Histologic studies of Placoderms and fossil Elasmobranchs. I: The endoskeleton, with remarks on the hard tissues of lower vertebrates in general. *Ark Zool* **2**, 321–454.

**Paukkonen K, Selkainaho K, Jurvelin J, Helminen HJ** (1984) Morphometry of articular-cartilage – a stereological method using light-microscopy. *Anat Rec* **210**, 675–682.

**Peignoux-Deville J, Lallier F, Vidal B** (1982) Evidence for the presence of osseous tissue in dogfish vertebrae. *Cell Tissue Res* **222**, 605–614.

**Poole AR, Pidoux I, Rosenberg L** (1982) Role of proteoglycans in endochondral ossification – immunofluorescent localization of link protein and proteoglycan monomer in bovine fetal epiphyseal growth plate. *J Cell Biol* **92**, 249–260.

**Poole CA, Flint MH, Beaumont BW** (1984) Morphological and functional interrelationships of articular-cartilage matrices. *J Anat* **138**, 113–138.

**Poole AR, Matsui Y, Hinek A, Lee ER** (1989) Cartilage macromolecules and the calcification of cartilage matrix. *Anat Rec* **224**, 167–179.

**Rosenthal O, Bowie MA, Wagoner G** (1941) Studies in the metabolism of articular cartilage. I. Respiration and glycolysis of cartilage in relation to its age. *J Cell Comp Physiol* **17**, 221–233.

**Schmidt WJ** (1952) Über die Verkalkung des Knorpelgewebes der Haie. *Z Zellforsch Mikrosk Anat* **37**, 377–388.

**Schumacher BL, Su JL, Lindley SM, Kuettner KE, Cole AA** (2002) Horizontally oriented clusters of multiple chondrons in the superficial zone of ankle, but not knee articular cartilage. *Anat Rec* **266**, 241–248.

**Stockwell RA** (1967) The cell density of human articular and costal cartilage. *J Anat* **101**, 753–763.

**Stockwell RA** (1971) The interrelationship of cell density and cartilage thickness in mammalian articular cartilage. *J Anat* **109**, 411–421.

**Stockwell RA** (1978) Chondrocytes. *J Clin Pathol Suppl (R Coll Pathol)* **12**, 7–13.

**Stockwell RA** (1983) Metabolism of cartilage. In *Cartilage* (ed. Hall BK), pp. 253–280. New York: Academic Press.

**Szarko M, Bertram JEA** (2007) Articular cartilage function and organization: integrating dynamic mechanics with cryopreservation effects. *J Morphol* **268**, 1140–1140.

**Szarko MJ, Bertram JEA** (2006) Freeze-thaw treatment alters articular cartilage dynamic behaviour. *Integr Comp Biol* **46**, E139–E139.

**Takagi M, Parmley RT, Denys FR, Yagasaki H, Toda Y** (1984) Ultrastructural cytochemistry of proteoglycans associated with calcification of shark cartilage. *Anat Rec* **208**, 149–158.

**Wilsman NJ, Farnum CE, Leiferman EM, Fry M, Barreto C** (1996) Differential growth by growth plates as a function of multiple parameters of chondrocytic kinetics. *J Orthop Res* **14**, 927–936.

**Wong M, Carter DR** (2003) Articular cartilage functional histomorphology and mechanobiology: a research perspective. *Bone* **33**, 1–13.

**Youn I, Choi JB, Cao L, Setton LA, Guilak F** (2006) Zonal variations in the three-dimensional morphology of the chondron measured in situ using confocal microscopy. *Osteoarthritis Cartilage* **14**, 889–897.